The problem of increasing the radiation resource of scintillation detectors for proton and ion colliders

L. N. Zaĭtsev
Joint Institute for Nuclear Research, Dubna

Fiz. Élem. Chastits At. Yadra **30**, 1292–1327 (September–October 1999)

It is shown that at energies of 2–14 TeV and luminosities of 10^{32}–$10^{34}\,cm^{-2}\,sec^{-1}$ the radiation loads on scintillators (PS) and spectrum-shifting light guides (WLS) begin to exceed the maximum permissible level, and the resource decreases sharply. Since it is impossible to improve the radiation hardness of PS and WLS by means of the traditional chemical and technological methods, a dilemma arises: either the PS+WLS system must be changed frequently, which is technically difficult and uneconomical, or a new concept must be adopted of the careful planning of the sequence of exposures and breaks during which the properties of the system are restored. If the recovery time (the break) is short, it will not affect the results of fundamental studies carried out by experimentalists. © *1999 American Institute of Physics.*
[S1063-7796(99)00505-7]

INTRODUCTION

Work on the DØ and CDF detectors at the Tevatron in the United States[1,2] and on the CMS, ATLAS, and other detectors at the Large Hadron Collider (LHC) at CERN[3,4] is actively proceeding. At energies of 2–14 TeV and luminosities of 10^{32}–$10^{34}\,cm^{-2}\,sec^{-1}$, the radiation loads in the elements of these detectors will reach 10–100 kGy per year. It is clear *a priori* that polymers (scintillators, light guides, insulation, etc.) cannot withstand such loads. Therefore, active searches have begun for new impurities, antiradiation additives, and matrix technologies which can increase the radiation hardness. Since it is impossible to increase the scintillator resource by a factor of 10 to 30 by means of traditional chemical and technological methods, new inorganic heavy crystals like BaF_3, CeF_3, and $PbWO_4$ have begun to be used, in the hope that they will display greater radiation hardness.

The situation described in Ref. 5 is indicative. Acrylic scintillators which had been used in a uranium calorimeter for several years displayed a decrease in their light yield by a factor of 2 and a decrease in their transparency by a factor of 3 after an integrated radiation dose of 50 Gy, which is two orders of magnitude lower than in tests performed on small scintillator samples. At first it was assumed that this effect was due to the radioactive decay of the uranium. It was later shown that photoradiation oxidation of the scintilators was mainly responsible. Light and radiation act as powerful catalyzers of radiation oxidation.

Other calorimeters, for example, ones using polystyrene scintillators, work for several years with practically no loss of resolution. This is due to the spontaneous recovery of the optical properties of scintillators and spectrum-shifting light guides, which cannot be controlled. For example, the ZDS calorimeter in the WA-98 experiment at CERN, used in a beam of Pb nuclei of energy 158*A* GeV, had a continuous irradiation resource of 5×10^6 sec. It was found that scintillators of granulated polystyrene prepared by casting under pressure or by the extrusion method have better recovery properties than all the other known scintillators. At a load of 2 Gy/h it was possible to use the calorimeter for three runs instead of a single one. Taking into account the time for the spontaneous recovery of the polymer properties in conjunction with the timing of irradiation runs and breaks is apparently the most effective method of extending the resources of organic materials.[8]

1. RADIATION LOADS

Radiation loads are usually measured as the energy deposited (the dose)[1)] per unit time, neglecting fluctuations in the sensitive volume of the material. The accuracy of calculating the radiation load depends on knowledge of the physical processes by which the radiation interacts with matter, the characteristics of the material, the detector geometry, how completely the radiation sources are accounted for, and how well the mathematical model corresponds to the real processes.[7,8] Let us consider the radiation loads for the example of the CMS setup. In Fig. 1 we show the typical geometry of a detector used at a collider. The vacuum chamber (1) in which the beam collision region is located passes along the cylinder axis. The vertex and other track detectors are located inside the inner cavity (2). It is necessary to have as little matter as possible in this cavity (0.1–$0.5\,g/cm^2$). Detector elements made of dense materials surround the inner cavity: electromagnetic and hadron calorimeters, the solenoid, and background-shielding elements (3). Muon and other chambers are located in the surrounding space (4), both near and far from the calorimeters. In addition, in a number of detector setups, for example, CMS[3] and ATLAS,[4] there are so-called forward calorimeters (5). Located in front of them are beam collimators (6), which are responsible for most of the energy release ($\sim$60%) and are strong sources of radiation.

Sources of radiation. The main sources of radiation in such detector setups are the following:

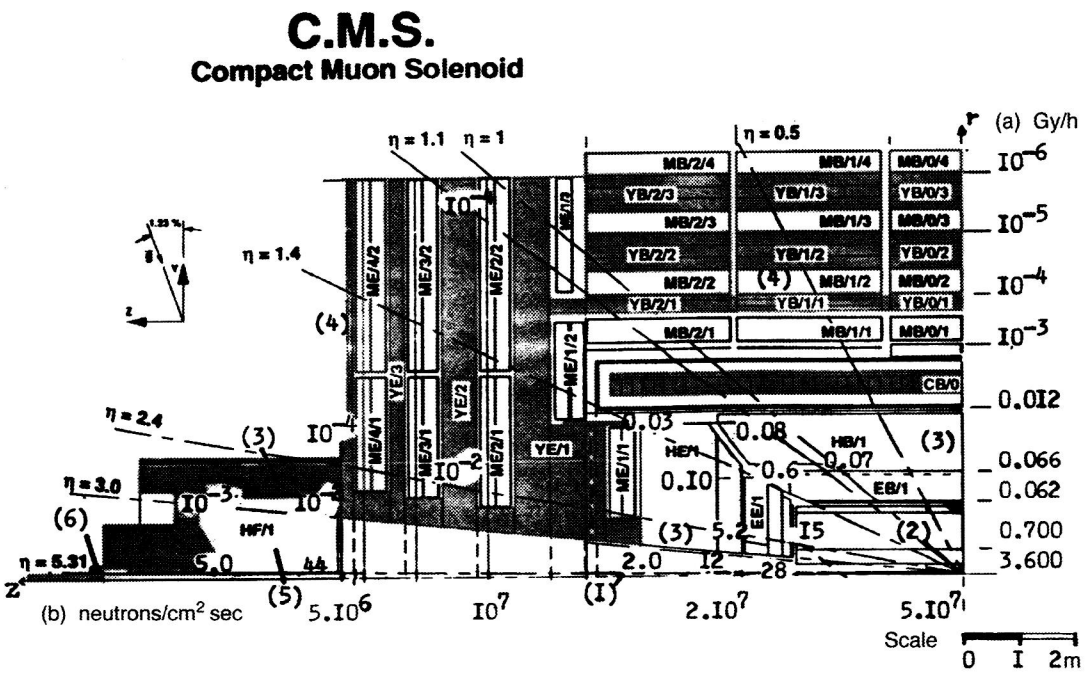

FIG. 1. Radiation load in CMS at $E_p = 14$ TeV, $L = 10^{34}\,\mathrm{cm}^{-2}\,\mathrm{sec}^{-1}$: (a) doses in one quarter of the cylindrical geometry; (b) neutron distribution in the vacuum chamber; (1)–(6) are explained in the text.

• direct radiation from *pp* (*AA*) collisions;

• radiation produced in the interaction of direct radiation with the vacuum chamber and the residual gas;

• radiation coming from dense materials in the inner cavity (the albedo);

• secondary radiation from interactions of the direct radiation and the albedo with materials inside the cavity (the chamber structures and detectors).

Initial estimates[9] of radiation loads usually took into account a single *pp* (*AA*) collision, determined by the secondary-particle multiplicity, and the unit of pseudorapidity η (Fig. 2) determined by the inelastic interaction cross section σ_{in} and the luminosity. Table I gives the particle yields in *pp* collisions at 14 TeV (Ref. 12).

In calculating the radiation loads due to particle interactions with the vacuum chamber, it is necessary to take into account the actual geometry, the dimensions of the collision region, the magnetic and electrostatic fields, the characteristics of the materials, and the spatial–angular and energy distribution of each type of particle in a *pp* (*AA*) collision.[10] Multiple Coulomb scattering, coherent and incoherent elastic nuclear scattering, the inelastic nuclear interaction, fluctuations in direct e^+e^- pair production, and so on, must be modeled in detail. The foundations for such modeling were first laid in Ref. 11, and later developed in Refs. 12–16.

The effect of the configuration of the vacuum chamber on the neutron yield was studied in Ref. 15. The magnetic field (4 T) was taken into account for the CMS detector.

The chamber configuration in the first 1.5–2 meters along the axis (Fig. 1) does not strongly affect the neutron yield. However, at distances of $\pm 2 \leqslant Z \leqslant \pm 15$ m the decrease of the neutron yield in relation to that in a chamber of constant cross section is quite significant (up to a factor of 5). The authors of the CMS study did not consider the formation of a linear source of all the particles and fragments, which is particularly important in *AA* collisions of heavy nuclei (where the vacuum chamber can be represented as an extended linear source of radiation[8]).

The locations of particle collisions with the chamber wall and the emission angles α_{E} were determined by a simi-

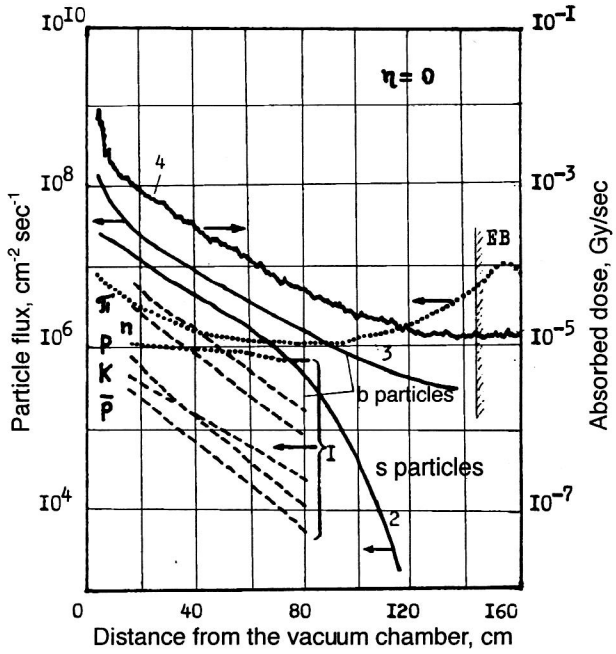

FIG. 2. Radial distribution of particle fluxes and the absorbed dose (load) in the CMS track region for $E_p = 14$ TeV, $L = 10^{34}\,\mathrm{cm}^{-2}\,\mathrm{sec}^{-1}$, $B = 4$ T (1–4 are explained in the text).

TABLE I. Particle yields from pp collisions at 14 TeV.

Type of particle	Percent per proton
p	0.98–1.98
η	1.14–1.88
K^+, K^0	7.42–8.01
$\pi^\pm$	34.8–39.8
Σ, Λ, ...	0.80–2.13
p, n, Σ, ...	2.91–5.82
$e^\pm$	0.50–0.55
γ	44.9–46.4

lar technique taking into account recent studies on the multiple production of α particles and fragments.[17,18] In Table II we show some characteristics of a uniformly distributed linear source within $Z=\pm 3$ m (Fig. 1), taking into account particles entering not only from inside the chamber, but also from outside it (the albedo) in the formation of the linear source. Particles of the leading group practically do not undergo inelastic interactions in the case of a chamber wall of thickness $d=0.15$–0.25 cm, both owing to the large mean free path λ_{in} before an inelastic interaction, and owing to the small emission angles $\alpha_E < 100\ \mu$rad.

The probability of a particle inelastic interaction in the chamber wall is

$$P=1-\exp(d/\alpha_E\cdot\lambda_{in}), \tag{1.1}$$

and the fraction of inelastic interactions is

$$\nu_*=1/\lambda_{in}\exp(-x/\lambda_{in}). \tag{1.2}$$

It is clear from (1.1) and (1.2) that for $r_a=6$ cm and $d=0.12$ cm, nearly 90% of all the interactions will be localized in the wall. In a grazing impact of a particle on a semi-infinite medium of aluminum with a vacuum–matter boundary, the number of inelastic interactions per primary particle with energy E_0 (in GeV) is given by

$$\nu_*=2AE_0^i+2.34\times 10^{-3}\ln(5E_0^j), \tag{1.3}$$

where $i=p,d,n,\pi,\ldots$ and $j=e^+,e^-,\gamma$, giving the reactions (γ,n_π), $(\gamma,n_{\pi\pi})$, (γ,nn), and so on. Owing to reflection, the value of ν_* is actually much smaller.[8]

In the case of CaCa and PbPb (Table II), the particle trajectories were not modeled; instead, the phenomenological method of "equivalent protons," first proposed in Ref. 23, was assumed valid (see below). Here the linear source in an AA interaction is determined from the expression

TABLE II. Linear source $2\pi r_a$, particles/cm^{2}sec^{-1} [r_a is the radius of the vacuum chamber, equal to 6 cm (A1), and $\langle E_0\rangle=6$ GeV corresponds to charged particles with $10^{-1}<\alpha_E<10$ mrad].

Particles giving ν_*	$\langle E_0\rangle$ (GeV)	Luminosity, cm^{-2} sec^{-1} 10^{34} (pp)	10^{29} (CaCa)	10^{27} (PbPb)
Σ	6	$8\cdot10^7$	$4\cdot10^7$	$6\cdot10^7$
$i\to p,\pi,e,\gamma$				
Neutrons	$\sim10^{-3}$	$3\cdot10^7$	$7\cdot10^6$	$5\cdot10^6$
No. of equiv. protons	-	$1.3\cdot10^{14}$	$6.7\cdot10^{13}$	10^{13}

TABLE III. Integrated luminosity and number of ions in the beam [LHC, 14 TeV; see D. Brandt *et al.*, LHC Note 264; the values of the equivalent protons are highlighted (our estimate)].

p	$1.2\cdot10^{34}$	$3.3\cdot10^{33}$	$1.5\cdot10^{33}$	$5.5\cdot10^{32}$	$1.1\cdot10^{32}$
	$1.3\cdot10^{14}$	**$6.8\cdot10^{13}$**	**$4.6\cdot10^{13}$**	**$1.7\cdot10^{13}$**	**$3.3\cdot10^{12}$**
$^4He_2$	$9.9\cdot10^{32}$	$2.9\cdot10^{32}$	$1.4\cdot10^{32}$	$5.1\cdot10^{31}$	$1.0\cdot10^{30}$
	$3.7\cdot10^{13}$	$2.0\cdot10^{13}$	$1.4\cdot10^{13}$	$3.5\cdot10^{12}$	$6.8\cdot10^{11}$
	$1.5\cdot10^{14}$	**$8.0\cdot10^{13}$**	**$5.6\cdot10^{13}$**	**$1.4\cdot10^{13}$**	**$2.7\cdot10^{12}$**
$^{16}O_8$	$2.9\cdot10^{31}$	$9.9\cdot10^{30}$	$5.0\cdot10^{30}$	$1.8\cdot10^{30}$	$3.6\cdot10^{29}$
	$6.3\cdot10^{12}$	$3.7\cdot10^{12}$	$2.6\cdot10^{12}$	$9.3\cdot10^{11}$	$1.9\cdot10^{11}$
	$1.0\cdot10^{14}$	**$5.9\cdot10^{13}$**	**$4.2\cdot10^{13}$**	**$1.5\cdot10^{13}$**	**$3.0\cdot10^{12}$**
$^{40}Ca_{20}$	$1.8\cdot10^{30}$	$6.9\cdot10^{29}$	$3.9\cdot10^{29}$	$1.4\cdot10^{29}$	$2.8\cdot10^{28}$
	$1.6\cdot10^{12}$	$1.0\cdot10^{12}$	$7.4\cdot10^{11}$	$2.8\cdot10^{11}$	$5.5\cdot10^{10}$
	$6.4\cdot10^{13}$	**$4.0\cdot10^{13}$**	**$3.0\cdot10^{13}$**	**$1.1\cdot10^{13}$**	**$2.2\cdot10^{12}$**
$^{97}Nb_{41}$	$6.4\cdot10^{28}$	$2.4\cdot10^{28}$	$1.3\cdot10^{28}$	$4.8\cdot10^{27}$	$9.6\cdot10^{26}$
	$3.3\cdot10^{11}$	$1.8\cdot10^{11}$	$1.3\cdot10^{11}$	$5.0\cdot10^{10}$	$9.6\cdot10^{9}$
	$3.2\cdot10^{13}$	**$1.7\cdot10^{13}$**	**$1.3\cdot10^{13}$**	**$4.8\cdot10^{12}$**	**$9.3\cdot10^{11}$**
$^{208}Pb_{82}$	$8.9\cdot10^{26}$	$2.7\cdot10^{26}$	$1.4\cdot10^{26}$	$5.1\cdot10^{25}$	$1.0\cdot10^{25}$
	$4.8\cdot10^{10}$	$2.0\cdot10^{10}$	$1.4\cdot10^{10}$	$5.3\cdot10^{8}$	$1.0\cdot10^{8}$
	$1.0\cdot10^{13}$	**$4.2\cdot10^{12}$**	**$2.9\cdot10^{12}$**	**$1.1\cdot10^{11}$**	**$2.1\cdot10^{10}$**

$$S_{AA}(Z)=A(N_p(L_p)/N_A(L_A))\times S_P(Z), \tag{1.4}$$

where N_p and N_A are the numbers of protons and ions in the colliding beams. In Table III we give the values of the equivalent protons for the CMS, ATLAS, and ALICE detectors at the LHC collider. We show the conventional boundary $\sim10^{13}$ equiv. protons, below which the radiation loads do not present any great problem for most materials used in detector setups. It is often claimed that the decrease of the luminosity by ~8 orders of magnitude, for example, from 1.2×10^{34} (pp) to 8.9×10^{26} (PbPb), *a priori* eliminates the problem of radiation danger. This is not true, because the number of equivalent protons is changed by only an order of magnitude, and it is this quantity which determines the internal radiation field, i.e., the radiation loads on the detector elements.

A surface source is defined by the albedo $i-j$, where i is a particle incoming from the medium and j is an outgoing one. The albedo is often expressed in percent and denoted by ξ_{ij}. The first estimates[19,20] confirmed the assumption of large albedos and stimulated the detailed study of this problem.[21,22] It turned out that the albedo plays an extremely important role in the inner cavity of a detector setup.[24,25]

As an illustration, in Table IV we give some values of

TABLE IV. Value of the albedo ξ_{ij} in % per proton incident on iron.[22]

Type $i-j$	Energy $E_{min}-E_{max}$, MeV	Energy E_p, GeV 1	10	70	200
$p-n$	10^{-3}–10^{-1}	9.0	85	230	540
$p-n$	10^{-1}–10^{3}	6.0	69	193	430
$p-p$	10^{-3}–10^{-1}	4.0	43	100	147
$p-p$	10^{-1}–10^{3}	1.0	27	3.5	11
$p-\pi$	10^{-1}–10^{3}	-	16	6.3	13
$p-\gamma$	10^{-1}–10^{-3}	3.0	20	15.5	32

TABLE V. Comparison of the radiation loads for CMS, in Gy/h (at $E=14$ TeV and $L=10^{34}$ cm^2/sec).

	Coordinates, cm (see Fig. 2)		ECAL		HCAL		ECAL	HCAL
η	r	Z	Ref. 3	Ref. 31	Ref. 3	Ref. 30	Our estimate	
		320	13	15			28	
		340						
3–2.8	40		**3.7**	**3**	**4.6**	**0.86**	**12**	**10**
		376						
		560			2.8	0.07		2
		320	8	6.5			15	
		340						
2.6–2.4	55		**2.8**	**1.4**	**4.5**	**0.13**	**5.2**	**5**
		376						
		560			0.9	0.01		0.4
	130	320	0.46	0.28			0.6	
		340						
1.5–1.4	↓		**0.09**	**0.03**	**0.04**	**0.02**	**0.08**	**0.07**
		376						
	286	560				10^{-3}		0.03
	130	145		0.2			0.22	
1.1–1	↓	206		**0.02**		**0.01**	**0.04**	**0.03**
	286	370				10^{-4}		0.014
	130			0.18			0.62	
0.1–0	↓	~0		**0.02**		$\mathbf{6\cdot10^{-5}}$	**0.06**	**0.065**
	286					10^{-6}		0.012

the albedo. We see that the main component of the radiation is neutrons, but the charged-particle yield is also significant, especially at low energies. For particles of energy less than 1 GeV incident on iron, the albedo is observed to depend strongly on the type of incident particle. As the energy increases, the dependence of ξ_{in} on the type of incident particle becomes weaker. This makes it possible to use the corresponding values of ξ_{pn} independently of the type of incident charged particle. The solution of the problem of the albedo contribution to the total radiation load requires information about the angular differential and energy differential distributions of the albedos of neutrons and charged particles. The calculation of the albedo due to events which have a very small probability of occurring makes the results obtained from programs for deep penetration (for example, FLUKA[16]) unreliable. Comparisons of the calculated values of the albedo with experiment[26,27] have not been made.

Dense materials. The following materials were first considered for the electromagnetic calorimeter (ECAL) of the CMS, labeled EE and EB in Fig. 1 (Ref. 25):

- scintillating CeF_3 crystals of density 6.16 g/cm^3;
- lead and liquid argon: a sandwich of 2 mm argon and 1.5 mm lead with average density 5.6 g/cm^3;
- lead and solid polystyrene (PS) scintillator: a sandwich of 4 mm polystyrene and 2 mm lead with average density 4.45 g/cm^3.

Later on, we will consider the possibilities offered by the use of $PbWO_4$ crystals instead of CeF_3 ones; this replacement does not strongly change the radiation picture.[28] The hadron calorimeter (HCAL, labeled HE and HB in Fig. 1) consists of layers of Cu (4 mm) and PS scintillator (10 mm) and has density 7.37 g/cm^3. Farther along the radius (Fig. 1) are the muon chambers and the "triggers" (ME and MB). In order to decrease the albedo of low-energy particles, at the EB and EE faces, and also between EB and HB, neutron-spectrum converters made of CH_2 of thickness 5 cm were used. The converter between EE and HE is 9 cm thick.

The radiation loads were calculated by means of the program of Ref. 16 with transformation coefficients for going from the particle flux to the dose of charged particles and neutrons.[29] The simplified geometry and also the representation of the real elements of the setup by a uniform mixture of heavy and light materials made it impossible to determine the actual dose in the sensitive volume (for example, in fibers of diameter 60 μm).

In Fig. 1 we show the distribution of the radiation load in the CMS detector, taking into account all the above sources of radiation in accordance with the data given in the last two columns of Table V. We note that both the preliminary estimates[3] and the calculated values in the technical plans[30,31] are much too low. Moreover, the calculations of the radiation loads in Refs. 3, 30, and 31 are not reliable, as they contain internal inconsistencies. For example, the numbers in boldface in Table V (the first four columns) cannot under any conditions differ in a row by more than 20%, because they refer to the same coordinates r and z of the physical setup (see Fig. 1).

The inner cavity. The vertex and other track detectors are located in the inner cavity. The track detectors can be made of scintillator wires (fibers) if they have acceptable

radiation resources. The radiation load is largely determined by the minimally ionizing particles.

The radiation load from minimally ionizing particles can be written as[32]

$$\dot{D}(r)=1.6\times 10^{-4}L\times\sigma_{\text{in}}\times n\times(dE/Dx\sin\theta)\times(\sin\theta/2\pi r^2), \quad (1.5)$$

where $L=10^{34}\,\text{cm}^{-2}\,\text{sec}^{-1}$ is the luminosity, $\sigma_{\text{in}}=85$ mb is the inelastic interaction cross section, and $n=7$ is the multiplicity per unit of rapidity η. The stopping power $dE/dx\sin\theta$ is 2 MeV/cm^{2}g for all particles emitted in the polar angle θ. The number of particles created in a single collision and passing through unit surface of a fiber is $n(\sin\theta/2\pi r^2)$. The factor 1.6×10^{-4} Gy·cm^2/sec comes from the transformation from the flux to the dose.

For a solenoidal magnetic field ($B=4$ T), Eq. (1.5) is changed:

$$\dot{D}(r,B)=\dot{D}(r)\left(2\langle n_c\rangle\int_{x_1}^{x_b}f(x')dx'+\int_{x_b}^{\infty}f(x')dx'\right), \quad (1.6)$$

where $\langle n_c\rangle=\sinh\eta_{\max}/\sinh\pi\eta$ is the average number of circuits (windings) of the charged particles in the rapidity range $0<\eta<\eta_{\max}$ for the track detector,[33] and $f(x)=x\exp(-x)$ is the transverse-momentum distribution of particles with $x=2p_t/\langle p_t\rangle=0.3B/\langle p_t\rangle$. The average particle transverse momentum is $\langle p_t\rangle\sim 0.55$ GeV, and it is practically the same for AA collisions. The first integral gives the relation between the diameters of the circuits touching the fibers (x_i) and those reaching the inner ECAL surface, i.e., $d=p_t/0.15B$. For $\theta=90°$ ($\eta=0$) the number of circuits must be very large. Taking into account particle decay inside the volume of the track detector ($\eta_{\max}$), we have $\cot\theta_d=(m_0/c\tau)\times(\sinh\eta_{\max}/0.15B)$, where θ_d is the maximum angle ($m_0\sim 0.14\,\text{GeV}/c^2$ and $c_\tau=7.8$ m for $\pi^{\pm}$). In Ref. 32 it was found that the angle θ_d varies between 76° and 27° for B between 1 T and 6 T in the rapidity region $\eta_{\max}=1.5$. The second integral in Eq. (1.6) includes short-range particles which are absorbed by the calorimeter.

The flux of minimally ionizing particles has been calculated in the same manner,[32] taking into account the magnetic field (curve 2 in Fig. 2). We see that in relation to the estimates[34] without the magnetic field (the group of curves 1), the fluxes $F(B)$ are increased at small r and sharply decreased for $r>80$ cm. In the group of curves 1 we give the data on the neutron fluxes without the albedo. When the albedo is taken into account, according to our estimates and the data of Ref. 35, the neutron distribution better corresponds to curve 3, increasing for $r\to 0$ and $Z\to 140$ cm. In the first case this is due to the additional contribution from the linear source (the vacuum chamber), and in the second it is due to the large albedo, despite the presence of the CH_2 converter. Low-energy charged particles (b particles) also arising from the linear source and the albedo contribute significantly to the total dose.

In Fig. 3 we show the radial distribution of the energy deposited in the wall of the vacuum chamber and in the inner detector with average density 0.5 g/cm^2. If we take into account the two radiation sources, linear $S(Z)$ and point (pp), the dose distribution is closer to $1/r$ than to $1/r^2$ as found in Ref. 25.

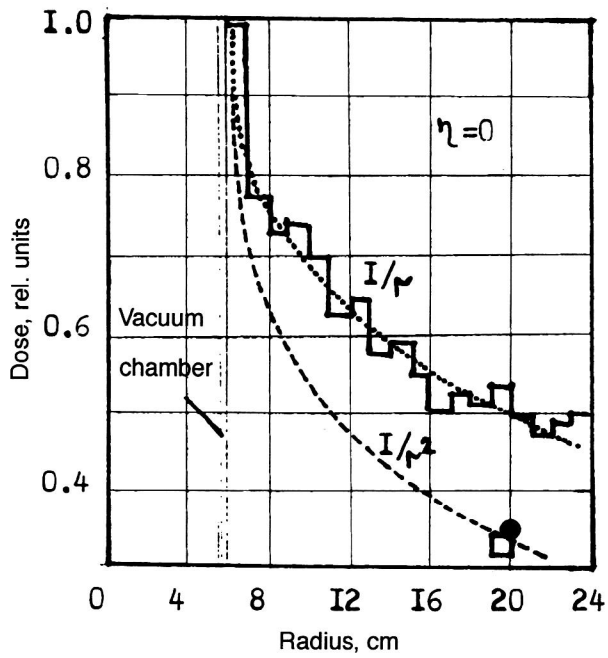

FIG. 3. Radial distribution of the radiation load near the CMS vacuum chamber. The broken line that looks like a histogram is our estimate from Ref. 8, and □ and ● are the estimates from Ref. 26.

The surrounding space. The main problem is to shield the muon chambers (Fig. 1) and the triggers from the background radiation composed of a broad spectrum of neutrons of energy ranging from 0.025 eV to several tens of MeV, and also γ quanta produced in neutron capture. The average energy of the captured γ quanta in iron is ~4 MeV (Ref. 8).

The first estimates of the composition and dimensions of the shielding for various detector setups used at colliders were made in Refs. 3, 4, 28, 30, and 31. The radiation environment of the CMS detector was studied in particular detail, and shielding materials were selected in Ref. 28. It was proposed that pure Pb and CH_2 be used at all collider setups. However, this is undesirable, as CH_2 is combustible and short-lived, while Pb is toxic. If Pb and CH_2 are incorporated in the coating of a special binding material such as polymer concrete, then not only is the manufacture of compact shielding greatly simplified and the aerosol danger decreased, but also the cost of the shielding is reduced.[36,37]

2. RADIATION RESISTANCE OF SCINTILLATORS AND SPECTRUM-SHIFTING FIBERS

In our review of the literature in this section we shall specially focus on the effects arising in the irradiation of scintillators and light guides at small loads and moderate doses, and the effects of reversible processes, spontaneous recovery, and so on. It is these effects which are important in practice, and they have not been well studied.

The limiting dose. The radiation sensitivity (radiation resistance) is primarily characterized by the limiting dose

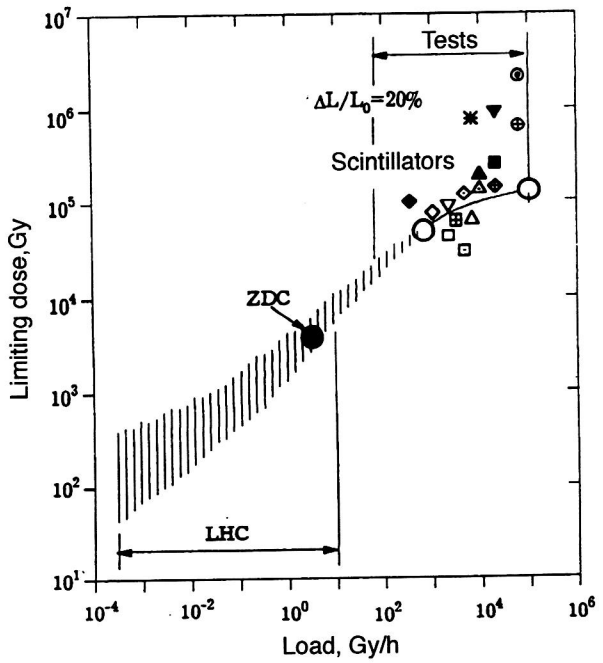

FIG. 4. Dependence of the limiting dose on the radiation load for loss of light yield $\Delta L'/L'_0=20\%$. The small points are for the "radiation-hard" scintillators of Ref. 46; ○ are for samples of standard PS1 scintillator; ● is for the real calorimeter ZDC;[69] and the shaded region is the estimate obtained by using the superposition method of Refs. 66 and 67.

D_{lim} for which the maximum allowed change of a particular optical property $\xi(D)$ of the material occurs.

The quantity D_{lim} is not universal. The interrelationship among the absorbed dose D, the dose rate D, the time of exposure to the radiation t_i, and the time τ and degree δ of spontaneous recovery is especially important.

An understanding of the nature of these dependences is of great practical value, for example, for predicting D_{lim} on the basis of accelerated radiation tests, since in such tests the dose rate, as a rule, does not correspond to the dose rate (the radiation load) under actual conditions of use (see Fig. 4).

The action of radiation at low doses of 10 to 10^4 Gy causes the optical emission spectra $d(\lambda)$, where λ is the wavelength of the light, to change. Changes in the spectra must not exceed 10–20% in real calorimeters, and so reversible processes dominate. Irreversible effects dominate for changes in the light yield by 40–60%. Here we shall mainly study reversible changes due to the formation of excited states of molecules of charged particles, free radicals, complexes with charge transfer, and so on.[38,39]

The quantitative description of radiation effects is based on the concept of the radiochemical yield:

$$G=f(D). \tag{2.1}$$

It is common to distinguish the initial yield G_0 for $D\to 0$ and the observed yield G of radiolysis products of the material, which indirectly characterizes the change of the amount or the properties of the matter for a given absorbed dose.[40]

It has been shown[41–44] that the nature of radiochemical processes at low doses is significantly affected by impurities in polymers, including oxygen and the residual monomer, which are preserved in the matrix structure. The radiolysis distribution over the sample volume is nonuniform, especially at low doses, and depends on the specific features of the absorption of ionizing radiation with the most dangerous, low values of the linear energy transfer (LET). Radiation effects at low doses have been less well studied experimentally, probably because investigators have primarily been seeking polymer properties which are easily measured.

At low dose rates the radical concentration increases linearly with the dose:

$$[R]=[R]_{\text{lim}}(1-\exp(-kD)), \tag{2.2}$$

where $[R]_{\text{lim}}$ is the limiting radical concentration, and k is the effective radical decay constant. At room temperature the constant k is about 10^3 Gy^{-1}, and the radical yield grows with increasing radiolysis temperature of polymers. On the other hand, results have been obtained which indicate that the radical yield and limiting concentration fall with increasing dose rate.[45] The radical yields also decrease with increasing LET, owing to the increase of the local radical concentration along the track and thus the high probability of recombination.[46]

In those cases where the free-radical recombination rate is comparable with the first-order reaction rates (associated with forming or breaking double bonds), the dependence of the radiation effects on the dose rate is very important, especially in chain reactions. Radiation- and photoradiation-induced oxidation, gas generation, and so on, occur via chain reactions.

In Fig. 4 we show the dependence of the limiting dose of scintillators on the radiation load (dose rate) over a wide range. The experimental data (points) are given for the best known scintillators. We note that the largest limiting doses are obtained for liquid scintillators under vacuum conditions (upper points in Fig. 4). In all cases, contact of the liquid scintillator with air leads to noticeable worsening of its luminescence and optical characteristics, even for dose rates as high as $5\times 10^3-10^4$ Gy/h (Ref. 46). The limiting dose was determined only for accelerated irradiations of small samples, mainly by low-energy α, β, and γ sources,[46–59] rarely ionizing neutrons,[60,62] and in beams of high-energy particles.[61,63,64] We see from Fig. 4 that the overwhelming majority of the results obtained earlier cannot give a correct prediction for the LHC detectors.[30,31] In order to obtain results for $D\leqslant 10^{-2}-10^{-3}$ Gy/h, it would be necessary to have 5–8 years of exposure, which is practically impossible.

A semiempirical model. The authors of Ref. 64 were the first to propose the use of the well known principle of temperature–time superposition,[65] where the exposure temperature and dose rate are related. It has been used successfully by nuclear power stations in the United States[66,67] for predicting the ageing of polymer electrical insulation of cables. In 1985 (see the Appendix in Ref. 64) this principle was used for a satisfactory description of experimental results. The semiempirical model is applicable to any polymer, including scintillators, especially at low doses where there are no phase transitions: vitrification, amorphization, and so on. Figure 4 gives the first illustration of the reproduction of the dependence $D_{\text{lim}}(D)$ in the range $10^{-4}\leqslant D\leqslant 10$ for scintillators.[60]

Let us discuss the essentials of the model. The analysis of a large amount of data allowed the authors of Ref. 68 to state that the free-radical ratio $G(300\,\mathrm{K})/G(T)$ decreases linearly with increasing temperature for any polymer. At higher temperatures accelerated radiation–oxidation ageing occurs without any change of the basic chemical-reaction mechanism, corresponding to the Arrhenius law:

$$v_k \sim \exp(-E/RT), \tag{2.3}$$

where E is the total, empirically determined activation energy, treated as the effective energy of the entire thermally activated process, v_k is the reaction rate, and R is the gas constant. To convert the results of the measurements obtained at higher temperatures to the conditions at the working temperature T_w, we use the shifting factor

$$\dot{a} = \exp(E/R(T_w^{-1} - T^{-1})). \tag{2.4}$$

The yields of products of radiation–chemical oxidation in the isothermal regime (250–400 K) are described by

$$G = k + A\exp(-E_1/RT)(G(R\cdot)/\dot{D})^{1/2}[RH], \tag{2.5}$$

where k is an empirical coefficient taking into account the formation of radiolysis products in radical recombination, A is the pre-exponential factor, E_1 is the activation energy of the process, which is usually close to the activation energy of an extended chain reaction (30–50 kJ/mole), $G(R\cdot)$ is the radiation–chemical yield of free radicals, and $[RH]$ is the concentration of oxidizable compound.

Photoradical chain reactions occur for $\Phi I \tau_r > 1$, where Φ is the quantum yield of radicals, I is the intensity of visible light, and τ_r is the radical lifetime. In the range from low to room temperatures, photoradical chain reactions occur at practically all values of Φ and τ_r if the intensity of visible light is greater than about $10^{13}\,\mathrm{cm}^{-2}\,\mathrm{sec}^{-1}$ (Ref. 39). The energy transferred by active particles to photoradiation processes due to the absorption of radiation at optical frequencies is

$$E_2 = \ni (G\dot{D}\tau_r) x I \varepsilon, \tag{2.6}$$

where $\ni$ is the extinction coefficient, x is the sample thickness and ε is the average photon energy. The energy entering via this channel can in some cases be comparable with or significantly greater than the energy entering due to ionizing radiation. This additional energy also goes into inducing chemical reactions. The activation energy in (2.4) is the sum of the two quantities $E = E_1 + E_2$ from Eqs. (2.5) and (2.6). Then the expression for the shifting factor takes the form

$$\dot{a} = A\exp(E/R(T_w^{-1} - T^{-1}))(G(R\cdot)/\dot{D})^{1/2}[RH]. \tag{2.7}$$

The region in the range of D from 10^{-4} to 10^{0} Gy/h (Fig. 4) was estimated by taking into account the additional activation energy E_2 of the process for light intensity of the radioluminescence $\sim 10^{15}\,\mathrm{cm}^{-2}\,\mathrm{sec}^{-1}$. This was the light intensity used in the CERN experiment at the real calorimeter ZDC.[61] For $D = 10^5$ Gy/h the first experimental point was obtained in 1986 at the linear electron accelerator in Kharkov for $E_{el} = 1.2$ GeV and flux 10^{11} electrons/cm^2 sec. The irradiation time was 10 h. The second point at $D = 10^3$ Gy/h was measured in 1992 at the JINR, using a ^{60}Co setup. The samples had dimensions $4 \times 150 \times 150\,\mathrm{mm}^3$ and were prepared by the same technology as for PS1 (see below; addition of 1.5% pTP + 0.03% POPOP + 1% antiradiation impurity). The experimental values obtained for D_{lim} were respectively 7×10^4 Gy and 1.2×10^5 Gy (Fig. 4). Such scintillators can really be termed radiation-hard.[59] However, in the irradiation of the same scintillators in the real lead calorimeter ZDC (10^{11} accelerated Pb nuclei of energy 158A GeV; Ref. 69), the value $D_{lim} = 4 \times 10^3$ Gy was obtained. The exposure lasted 1.4×10^3 hours in the presence of atmospheric oxygen, and the dose rate was ~ 2 Gy/h. This large difference between the values of D_{lim} for small samples and the calorimeter can be attributed to (a) photoradiation oxidation (due to the different values of D), (b) the difference of the scintillator sizes and the presence of light guides made of polymethylmetacrylate (PMMA), and (c) the LET effect, equal to ~ 0.2 keV/μm for ^{60}Co and 20 keV/μm for a mixed radiation field.

For $D > 10^2$ Gy/h (see Fig. 4), when the value of the load is "equivalent" to the vacuum conditions, the dependence of the radiation-induced changes on the dose rate is weaker (and sometimes even absent). Therefore, at large D, and also for sufficiently thick samples, conditions arise in which only the surface layer is oxidized, while the bulk of the polymer is not.

Owing to the nonuniformity of the radiolysis process even in a single-phase system, there is always a flux of radiolysis energy toward the surface. Therefore, polymers can be viewed as heterogeneous.[70] Single crystals with defects, for example, $PbWO_4$, can also be regarded as heterogeneous systems in this sense.[71]

A uniform distribution of optical density throughout the volume is observed in PMMA irradiated *in vacuo* (Fig. 5, curve 1). If the irradiated polymer is stored in air, then, along with gas diffusion from the sample, there is diffusion of atmospheric oxygen inside the sample. The oxygen accelerates radical "decay" and thereby affects the formation of the spatial distribution of the optical density, which takes the form shown by curve 2 (Ref. 72). The same picture is observed when scintillators are irradiated in air.

The radiation-induced degradation of the polymer properties depends weakly on D below 10^{-2} Gy/h. Limiting doses D_{lim} significantly smaller than in the case of high dose rates are always observed (Fig. 4). This implies that the radiation-oxidation transformation occurs nearly throughout the volume of the polymer. The polystyrene initially acquires a two-layer structure, owing to the strong oxidation of the surface layer and weak oxidation of its bulk, which is deprived of oxygen as a result of the limitations on diffusion. The time for structural relaxation can reach tens or hundreds of days at room temperature, i.e., it significantly lags that of chemical transformations.

As a result, in such a material of inhomogeneous composition the mechanical stresses tend to grow, leading to the formation of microscopic cracks. These cracks act as channels along which oxygen (or ozone) from the surrounding air enters the interior of the sample, leading to rapid radiation ageing of the polymer.

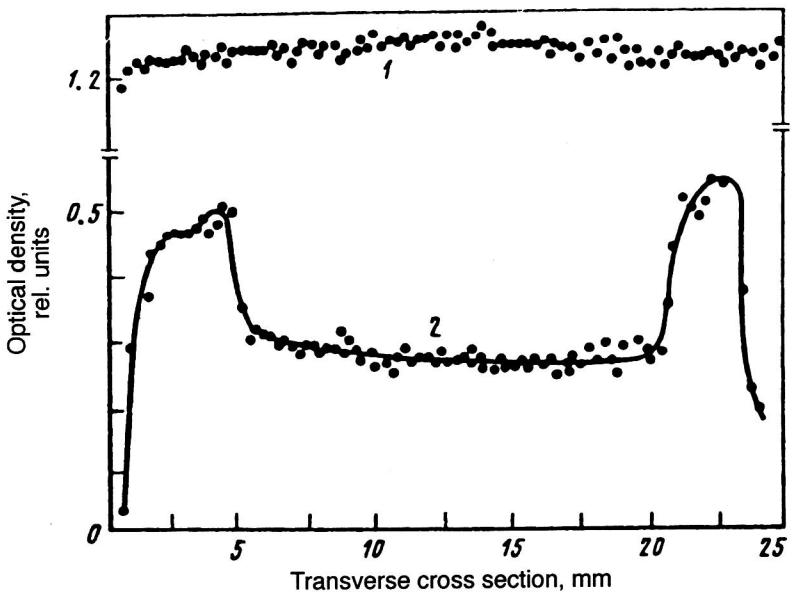

FIG. 5. (*1*) Optical density in the transverse cross section of a PMMA sample irradiated *in vacuo* to a dose of 30 kGy, and (*2*) the same after storage in air for 30 days.[72]

At dose rates in the intermediate range $10^{-2}<\dot{D}<10^{2}$ Gy/h (Fig. 4), the limiting dose has the following $\dot{D}$ dependence:[64]

$$D_{\lim}\approx D_0(\dot{D})^n, \tag{2.8}$$

where n characterizes the approximate linear dependence $\log D(\xi)=f(\log \dot{D})$, which can be determined only from experiments.

The role of the LET. Molecular ionization and excitation processes play a fundamental role in the radiation-induced changes of polymer properties. Elastic nuclear collisions can dominate at low velocities of heavy charged particles when $v_u/v_0\approx 0.6$, where v_0 is the electron Bohr velocity.

We see from Table VI that equal LETs on tracks of ions with different charges occur at different ion velocities.[73] Since the effective track radius increases with increasing ion velocity, in the case of α particles the absorbed energy is distributed in a track of large volume. As a result, the local and average yields of active particles will be lower for an ion with larger charge and mass. Therefore, G does not depend directly on the LET. Accordingly, the authors of Ref. 73 proposed a model for describing radiation-induced transformations using the charge and velocity of the charged particle. The observed increase of the PS degradation upon irradiation in a hadron field, in comparison with a γ field, lies within the error.[64]

The ratios G_D/G_C in PS and PMMA irradiated by γ rays and fast neutrons ($\dot{D}\sim 10^2$ Gy/sec; $T\sim\kappa$) differ very little in the presence of atmospheric oxygen, but differ *in vacuo* by a factor of 5 to 10 (Refs. 74 and 75). The effects of electrons (2 MeV), protons (8 MeV), α particles (30 MeV), and C^{4+} and N^{4+} ions (80 MeV) on the mechanical properties of aliphatic polymers have been compared.[76,77] Chromatic film dosimeters made of polychlorstyrene (analogous to FWT-70 used abroad[79]), carefully calibrated in various radiation fields, were used in Refs. 61 and 78 (Table VII).

In Fig. 6 we show the doses $D_{\lim}$ producing an increase

TABLE VI. Characteristics of proton and α-particle tracks at various values of the LET in polystyrene.

	98 keV/μm		50 keV/μm	
Characteristic	Protons	α particles	Protons	α particles
Energy, MeV	0.082	4.5	0.4	10
Velocity, v, cm/sec	4	15	8.7	22
Effective charge	0.69	2	0.93	1
Average number of electrons ejected by an ion over 1 nm of track length	1.56	1.7	0.86	1
$E_{\max}$ of δ electrons, keV	0.181	2.5	0.86	5.45
Core radius, nm	1.2	4.5	2.65	6.7
Effective track radius, nm	2.5	21	6.0	35
Energy transported by δ electrons beyond the track core, keV/μm	4.3	16.3	7	12.4
Average density of ionization events in the track core, 10^{20} cm^{-3}	5.3	0.45	0.69	0.1

TABLE VII. Sources of irradiation of polychlorstyrene samples.

Irradiation site	Types of particle (i—primary; j—secondary)	Dose rate D, Gy/sec	LET, keV/μm
(●) Channels of the IBR-2 reactor, JINR	$\gamma_i, n_i \rightarrow \gamma_j$, $E_n > 1$ MeV, $4.2 \cdot 10^{12}$ n/cm^{-2} sec	$5.8 \cdot 10^3$	60
(△) Copper target; 70-GeV synchrotron, IHEP	Various spectra $p_i \rightarrow (p,n,e^{\pm},\pi^{\pm},\mu\ldots)_j$	$2.5 \cdot 10^{-1}$	15
(▲) Exit window of the 650-MeV phasotron, JINR	$E_p = 650$ MeV, 10^{12} $p/\text{cm}^{-2} \cdot$sec	$2.9 \cdot 10^2$	8
(○) Copper target; 7-GeV synchrotron, ITEP	Various spectra $p_i \rightarrow (p,n,e^{\pm},\pi^{\pm}\ldots)_j$	$7 \cdot 10^{-2}$	9
(◆) Gamma setup	$E_\gamma = 1.25$ MeV	30	0.2

in the optical density of polychlorstyrene and also an elongation of polyethylene. Despite the fundamentally different parameters ξ_{lim} in the two materials, the radiation damage tends to decrease as the LET increases. This suggests that radiation-induced transformations have the same nature in essentially different polymers.

The review of Ref. 80 is devoted to the formation of stable radiolysis products as a function of the type of radiation. Comparison of G_D/G_C, on the one hand, and the yield of stabilized radicals, on the other, in irradiation by α particles and γ rays has shown that there is no correlation between the yields and the LET for most polymers. The rates of other, little-studied reactions may be increased significantly in the radiolysis region. This can be explained by invoking the microdosimetry concept,[81] and also by taking into account the contribution of energy scattering in elastic collisions. Processes involving the formation and decay of unsaturated bonds, radiation-induced oxidation, and also the behavior of polymers with changing temperature as a function of the particle type (the LET) remain unstudied.

Spontaneous recovery. The scintillator most widely used in Russia is the polystyrene PS matrix, in which first the scintillation impurity pTP and, second, the spectrum-shifting impurity POPOP are dissolved. In the first stage of the interaction of ionizing radiation, excitation of the matrix occurs and is transferred in a radiationless manner to the first impurity, and then in a radiation manner from the first to the second impurity. The second impurity shifts the spectrum to high transparency of the matrix or optimal sensitivity of the photoreceiver.

As can be seen from Fig. 4, investigators have endeavored to create scintillators which withstand a limiting dose $D_{\text{lim}} > 10^5 - 10^6$ Gy for a light yield $\xi_{\text{lim}} \sim 80-90\%$ after irradiation. The basic stages in this area of studies of the last few years were formulated in Ref. 60: (1) choice of the primary impurity; (2) choice of the secondary impurity; (3) the use of antiradiation impurities; (4) improvement of the matrix structure; (5) acceleration of recovery processes (how is not indicated).

The first four stages have not turned out to be very promising.[63,82]

It has proved impossible to increase D_{lim} to more than 10^5 Gy even for $D > 10^2$ Gy/h. Antiradiation impurities have proved ineffective at low D, i.e., for strong photoradiation oxidation. It is absolutely unrealistic to increase the D_{lim} of organic materials or polymers from 10^3 to the radiation loads of $10^5 - 10^6$ Gy which will be encountered at the LHC (see Fig. 4)! It is well known that a decrease of the number of

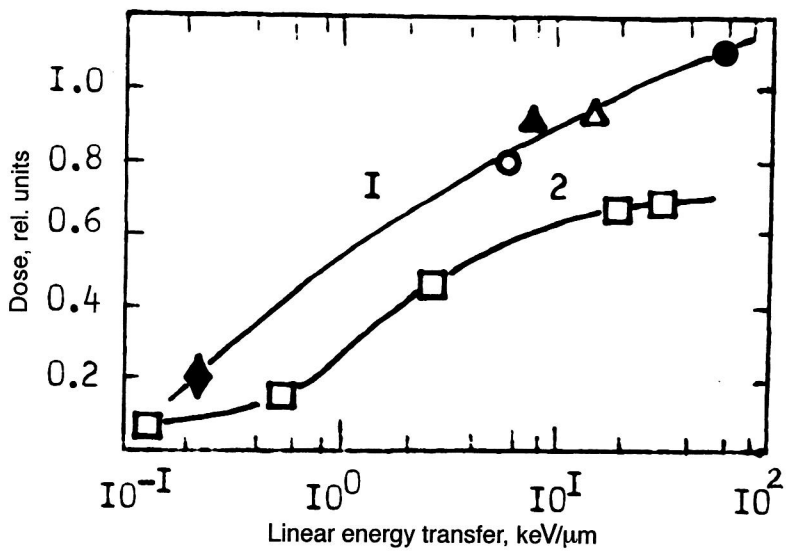

FIG. 6. LET dependence of the doses producing equivalent changes of ξ (see the text): (*1*) polychlorstyrene (the points correspond to the notation of Table VI); (*2*) polyethylene.[77]

TABLE VIII. Irradiation* and recovery parameters of several scintillators.

Material \ Parameter	No. of cycle	t_{ir}, h	D, kGy	τ, h	ξ, %	δ, %	$D_{lim}(\xi)$, kGy ($\xi=80\%$)
PS+2% pTP	1	56	28	480	92	97	20
+0.02% POPOP+0.01ST24	2	56	28	480	88	91	21
+20% UD7 (Ref. 82)	3	56	28	480	75	85	7
PSM-115+1.5% pTP	1	2	0.1	40	98	100	-
+0.05% POPOP							
+20% 1MN (Ref. 63)	2	20	10	72	90	110	25
NE-110** (Ref. 84)	1	120	26	500	90	92	30
SCSN81+1% PHB	1	56	28	316	85	22	24
+0.02% TBBT	1	68	34	500	60	65	24
+0.01% ST*** (Refs. 82 and 84)	1	200	100	600	45	48	24
PMMA+0.5%+	1	157	34	552	80	82	20
0.01% POPOP (Ref. 84)	1	463	400	552	48	48	20

*$\dot{D}=216-510$ Gy/h; ^{137}Cs and ^{60}Co γ sources.
**Nuclear Enterprise Company, Edinburgh, Great Britain.
***Kuraray Company, Tokyo, Japan.

chemical transformations by radical capture for non-chain reactions is impossible, because in radical capture by acceptors (antiradiation impurities) the number of products formed is roughly the same as in the absence of the acceptor, although their quantitative content is slightly changed.[83] A significant fraction of the radicals is produced along the particle track very close to each other, and they react quickly with each other. This process can be prevented only by creating very high concentrations of antiradiation impurities, which leads to unsatisfactory initial properties of the scintillators. Moreover, owing to the weak selectivity of radiolysis and the large number of different reactions occurring in photoradiation oxidation, it also is impossible to construct a single activity series of the antiradiation impurities.

When scintillators and light guides are used under real conditions, a series of limiting doses D_{lim} will be accompanied by periodic breaks during which the properties of the materials are restored.[84] Unfortunately, investigators have not caught on to the promise that this approach holds (see the following section), and have spent a great deal of effort on the useless search for scintillators which are radiation-hard under the conditions of continuous irradiation at high doses.

The data on the values of τ given in Refs. 58, 63, 82, and 84–90 vary considerably: from 103 days to 20–25 days. It should be noted that the different degrees of recovery δ of the optical properties depend mainly on the size of the dose: $\delta=40-70\%$ for $D\sim100$ kGy, $\delta=80-95\%$ for $D\sim10$ kGy, and $\delta\sim100\%$ for $D\sim5$ kGy. In the first two cases the values of ξ exceed the allowed ξ_{lim} by so much that it is difficult to compare the results.

In Table VIII we give the compositions and irradiation and recovery parameters of several scintillators. We see that the scintillator made of granulated polystyrene[91] PSM-115, produced by casting under pressure or extrusion,[92] is preferable in all its parameters. The data of Ref. 93 suggest a decreased yield of G radicals at high pressures. A satisfactory explanation can be obtained in terms of the thermodynamical free volume.[94] The free volume is decreased as a result of better packing of the macromolecules, a greater degree of crystallization, and so on, and so the probability for the appearance of radicals is decreased, while the recombination (decay) probability increases.

Recovery processes in spectrum-shifting fibers are much less well studied, and the results are very contradictory. The fibers BCF91A, Y11, and others irradiated by ^{60}Co and $n\gamma$ radiation from a nuclear reactor have been studied.[95] At a dose (^{60}Co) of 1.4 kGy ($D=5.5$ Gy/h), the light losses over a length of 1.5 m of fiber (diameter 1 mm) were respectively 10% and 15% for Y11 and BCF91A, and after 90 days the recovery was $\delta=98\%$. For an $n\gamma$ dose of 10 kGy ($D=1.5\times10^3$ Gy/h), the light losses reached 70–80%, and no recovery at all was seen after 20 days.

The conversion efficiency of these (and other) fibers after irradiation by ^{137}Cs ($D=216$ Gy/h) was studied in Ref. 63. One of the results for BCF91A is shown in Fig. 12. The smallest light losses over a length of 1.8 m (diameter 1 mm) were obtained for Y7, Y8, and BCF91A. The authors did not study the recovery in detail, but they state that after a dose of 20–36 kGy it was small (up to 20%) for $\tau=70-150$ h. However, upon irradiation of the calorimeter module made of Y7 fibers by an electron beam with $E=1.2$ GeV ($D=1.5\times10^5$ Gy/h), the light yield was reduced after a dose of 12.5 kGy to 0.4, and after 9 days it had recovered by 60% (to 0.65). The energy resolution was reduced from 5.4% to 18.2% (Ref. 96).

Our preliminary measurements of the optical density of BCF91A fiber[98] showed 100% recovery after a dose of 4.8 kGy ($D=1.4$ Gy/h), with recovery function of the form

$$d=d_0(1-a\exp(-t/b)), \tag{2.9}$$

where d_0 and d are the optical densities before and after recovery, and the constants are $a=0.16$ and $b=82$ h. In measuring $d(\lambda)$, where $\lambda=425$ nm, small changes of the fiber transparency after irradiation are not manifested in the region of the shifted spectrum.[96] The shifting impurity in BCF91A is a radiation-hard compound. The path length of

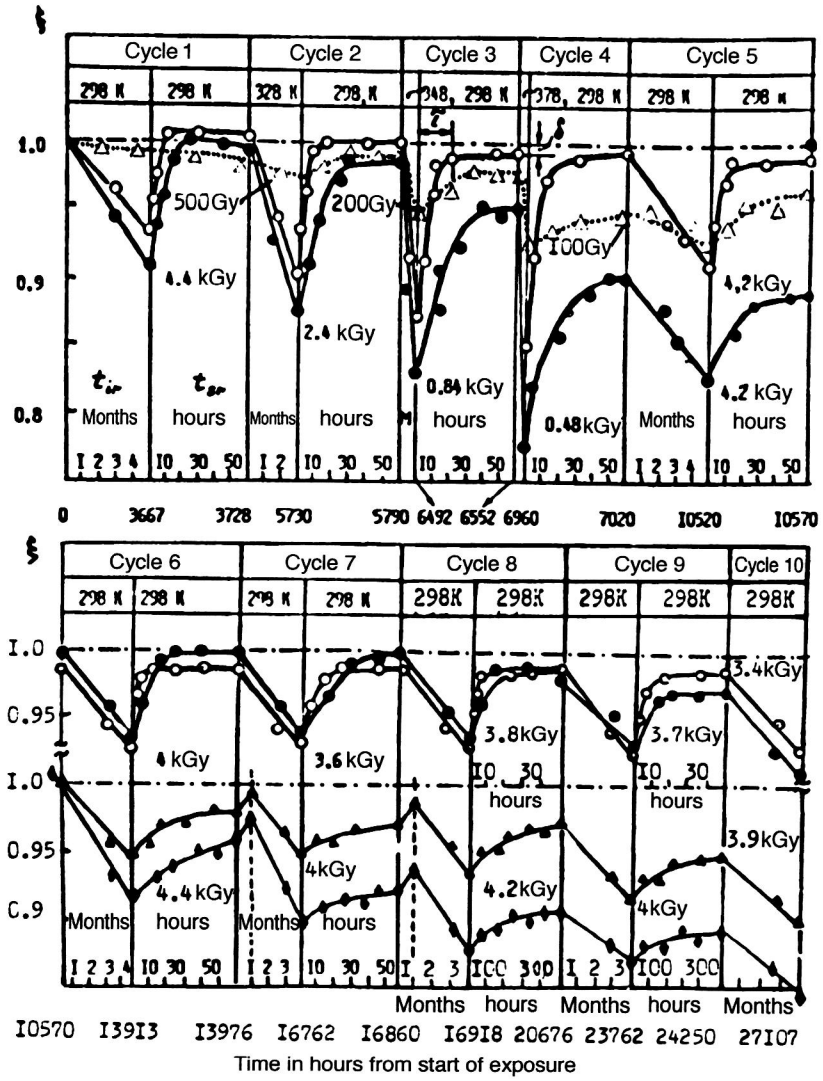

FIG. 7. Cyclical irradiation and recovery of scintillator samples (● PS1, ○ PS2, ▲ SCSN,[81] ◆ BC404A) and spectrum-shifting wires (△ BCF91A).[78,98]

the incident light before absorption is several μm. In the light-collection process, the path traveled by photons along the light guide can reach more than 2 m, and even small changes of the transparency can decrease the path length l by many times. It is therefore necessary either to measure $d(\lambda)$ at various λ, or to characterize the effect of the irradiation by the value of l and measure it by the technique of Ref. 97.

However, a more reliable method is to subject the calorimeter modules to radiation tests with the simultaneous cyclical irradiation of the scintillation plates and spectrum-shifting fibers. Identification of the dose rate in the tests and of the radiation load during use become important here, along with limiting the dose (per cycle) so as to prevent irreversible processes from occurring in the scintillators.

Cyclical irradiation. Under real conditions of calorimeter use, scintillating plates and fibers will be repeatedly subjected to radiation with some breaks between exposures. However, only double[82] and triple[63] irradiation cycles have been studied for PS scintillators (see Table VIII). Up to now no cyclical irradiations of spectrum-shifting fibers have been performed.[2)] Only multiple cyclic irradiations can help to understand the photoradiation-induced ageing of scintillators and fibers.

Observations of the photoradiation ageing of PS over the course of three years were first made in Refs. 78 and 98, using the techniques of Ref. 63 (Fig. 7). A heightened impurity concentration of ~3% pTP+0.04 POPOP was necessary to obtain the minimal time resolution[99] and to ensure shielding from matrix degradation.[100] Photostabilizing (0.05%) and antioxidation (0.05%) impurities like CCB[40] were added to PS2. They had practically no effect on the original characteristics of the PS2. Samples of PS were cut out from plates prepared by casting under pressure, using granulated polystyrene of brand PSM-115. Later on,[98] after five irradiation cycles of PS1 and PS2, observations of the ageing of SCSN81 (Kuraray, Japan) and BC 404A (Bicron, USA) were begun.

For this purpose, ^{137}Cs sources of low activity were placed between the samples, as shown in Fig. 8. A chromatic film dosimeter (CFD) was also located between the samples. The calibration of these dosimeters was mentioned above in Sec. 2. The dose distribution in the samples over the spectra of all the particles emitted by ^{137}Cs was calculated. The re-

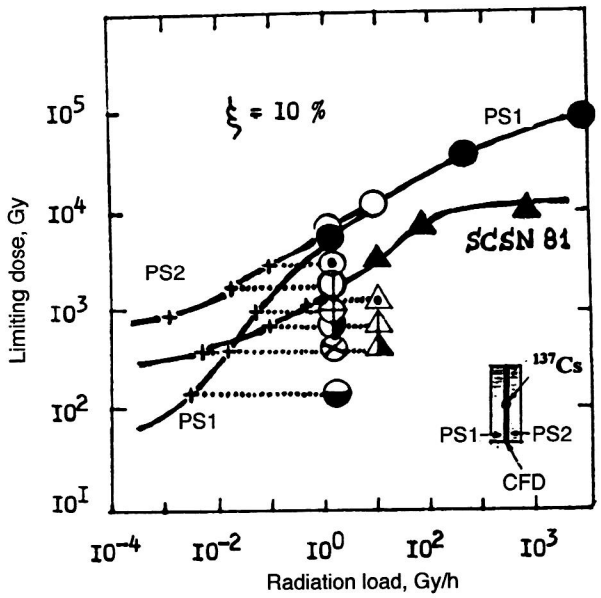

FIG. 8. Dependence of the limiting dose for light losses $\xi=10\%$ on the dose rate:

PS1	●	298K	⊕	328K	⊗	348K	◒	378K
PS2	○		◑		⊖		⊙	
SCSN81	▲	300K	△	315K	⧋	335K	◭	350K.

sult was $D_{max}=1.2\pm0.14$ Gy/h (PS1 and PS2) and $D_{max}=1.4\pm0.12$ Gy/h (SCSN81 and BC404A).

In accordance with the recommendations of Ref. 96, only a single quantity was measured, the optical density $d(\lambda)$, by means of two spectrophotometers. The convenience of using the value of $d(\lambda)$ is obvious. It quantitatively characterizes the light absorbed by the sample, independently of the channels via which the excitation is dissipated. The effect observed as the change of $d(\lambda)$ after irradiation must be manifested more clearly in the emission spectra $E(\lambda)$. The error in measuring the optical density was less than 0.2%.

The emission spectra in all the samples were measured "episodically" only in order to monitor the dynamics of the process. As an example, in Fig. 9 we show the spectrum $E(\lambda)$ measured by the technique of Ref. 100 in a special (5 μm) PS2 sample. A mercury lamp was used to excite the fluorescence. The probability of absorbing the radiation of the first impurity (pTP) by the second one (POPOP) is small if the sample thickness is several μm (Refs. 101 and 102).

To understand fully the radiation processes, it is insufficient to measure the absorption spectra;[103,104] the emission spectra are also needed. Under very rapid changes $d(\lambda_{max}) \rightarrow (a+b)$, where $\lambda_{max}=425$ nm, light emission and transmission effects cannot be separated, but it is possible to make relative comparisons. At low doses (up to 5 kGy) there is, as a rule, no shift of λ_{max} or deformation of the spectrum; only the value of $d(\lambda_{max})$ changes, where $a \gg b$ for $T=298$ K. This implies that radiation-induced coloring of polystyrene is manifested more strongly than reduction of the light yield.[82]

The semiempirical model described in Sec. 2 above was first used to predict[98] D_{lim} at the very low D characteristic of

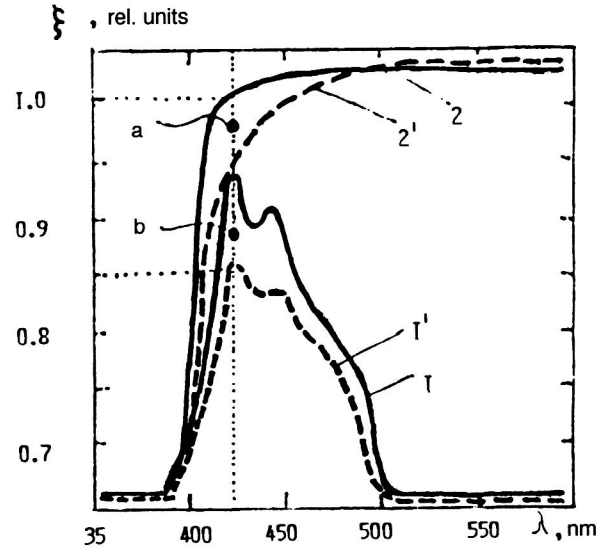

FIG. 9. Fluorescence ($1,1'$) and transmission ($2,2'$) spectra, respectively, before and after irradiation by a dose of 2.4 kGy at $T=328$ K of a PS2 sample (after recovery, the spectra coincide with *1* and *2*).

the LHC (see Figs. 4 and 8). We see in Fig. 7 that the standard PS1 sample recovers well at 298 K (the first cycle), but is strongly degraded with increasing temperature, despite the significant decrease of the dose (the second and fourth cycles). As expected, the PS2 sample containing antioxidant recovers its optical properties much more completely and rapidly. After more cycles (5–9) the stability remains unchanged after the third increase of the irradiation temperature. This effect is explained by the dominance of reversible processes in PS2 (Ref. 40):

$$RH \rightarrow R\cdot + H,$$

$$AH + R\cdot \rightarrow A\cdot + RH.$$

The antioxidant AH (of the CCB type) transfers an H atom to a free radical R·, transforming it into a less active radical and regenerating the original molecule. The ease of the H-atom transfer is due to the high stability of the radicals formed, owing to the steric screening of the oxygen atoms.

In the sixth cycle the PS1 sample was replaced by a new one in order to continue the observation of the photoradiation-induced ageing at $T=298$ K. For this purpose, SCSN 84 and BC 404A were irradiated at low doses. We see from Fig. 7 that these samples have very large values of δ and τ, i.e., their recovery is slow and incomplete. This is consistent with the earlier data (see, for example, Table VIII), but there is no explanation of these effects in the literature. Figure 10 was constructed from the experimental data of Refs. 78 and 98. It displays the time variation of the light yield (the dependence on the number of cycles) and is needed for determining the radiation resources of scintillation detectors.

3. DETERMINATION OF THE DETECTOR RESOURCE

When there are strict limits on the light loss (10–20%), organic scintillators and spectrum-shifting fibers do not withstand radiation loads of 50–100 kGy over a period of 10

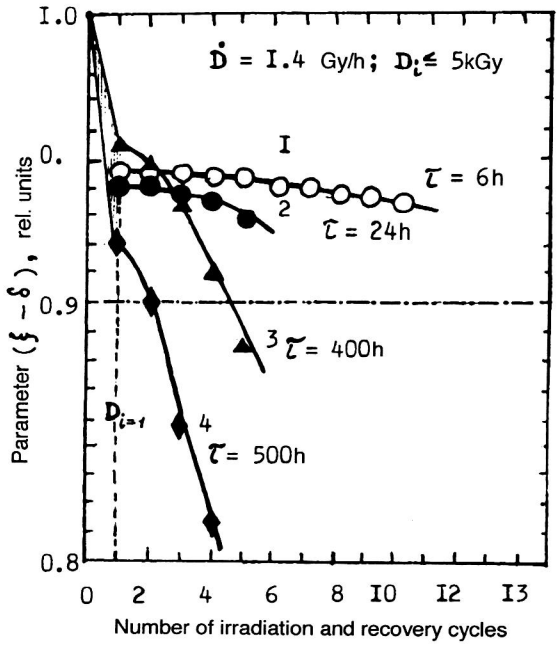

FIG. 10. Variation of the relative light yield, taking into account recovery (the parameter $\xi-\delta$; see Fig. 7), as a function of the number of cycles (the cycle time is $t_{ir}+t_{sr}\sim 4$ months): ● PS1, ○ PS2, ▲ SCSN81, ◆ BC404A.

years of use (total exposure time $\sim 10^8$ sec). The ideas discussed in Ref. 60 turned out to be unrealized, and so three alternative directions have recently been formulated:

- the development of new organic silicate scintillators which are stable with respect to radiation under conditions of continuous exposure;[105,106]
- radiation studies of liquid scintillators in quartz capillaries with periodic renewal of the scintillator;[46,95]
- study of the photoradiation-induced ageing and the spontaneous recovery of ordinary plastic scintillators containing new additives.[6,78]

In principle, all these approaches can significantly increase the radiation resource of scintillators, but exploratory studies as difficult as those described in Ref. 60 are required. For example, when using organic silicate scintillators for track detectors it is necessary to find additives which ensure a higher light yield. The large luminescence time (11–13 nsec) limits their use to high-load conditions. In addition, in some organic silicate scintillators, migration of luminophores to the surface is observed, where they are subsequently crystallized out. It is not surprising that up to now organic silicate scintillators have not been widely used in practice. As far as liquid scintillators in capillaries are concerned, they withstand large radiation loads only in a vacuum (Fig. 4) or a neutral medium, and this considerably complicates the detector construction. The third possibility, as we shall see below, offers the most effective way of increasing the detector resource, since it does not require that the materials have high radiation stability.

The technique. The resource of continuous irradiation determining the duration of a run is

$$t_r=k_3(D_{\rm lim}(\xi)/\dot{D}), \tag{3.1}$$

where $D_{\rm lim}$ is the limiting allowed radiation dose for $D \geqslant 10^2$ Gy/h, ξ is the defining parameter (the light yield L, light attenuation length l, optical density d, number of photoelectrons, and so on), and K_3 is the uncertainty coefficient (the allowance). In Table IX we give the coefficients K_3 for several scintillators, calculated in accordance with Figs. 7 and 8.

The radiation resource with breaks determining the working time is

$$t_R=f(D_{\rm lim},\dot{D},T,\tau,\delta,\xi\ldots), \tag{3.2}$$

where τ and δ are respectively the time and degree of recovery, and T is the temperature. Other factors like the corrosiveness of the medium, a magnetic field, and so on, can also affect t_R.

The HCAL resource. The accuracy of determining the resource is equally affected by how reliably the limiting allowed dose and the radiation load are determined. In Fig. 11 we give the radiation loads in the HCAL of the CMS obtained by various authors (see also Table V). We see that at present the values are completely unreliable. It is therefore absolutely necessary to take into account the uncertainty coefficients in calculations. The tendency for the HCAL collaboration[30] to underestimate the risk in order to find financial backing for their project is understandable, but at least the HCAL loads should be consistent with the ECAL loads[31] in those elements where they must certainly coincide.

In Fig. 12 we show the original experimental data.[30] The HCAL resource was estimated by using the upper boundary of the shaded region (3), although it would be reasonable (in the allowance) to take the lower boundary. Curve 2 in Fig. 13 is too low by a factor of 2.3, but this can be corrected. The main problem is that the results of accelerated tests (Fig. 12) have been incorrectly applied to operating conditions

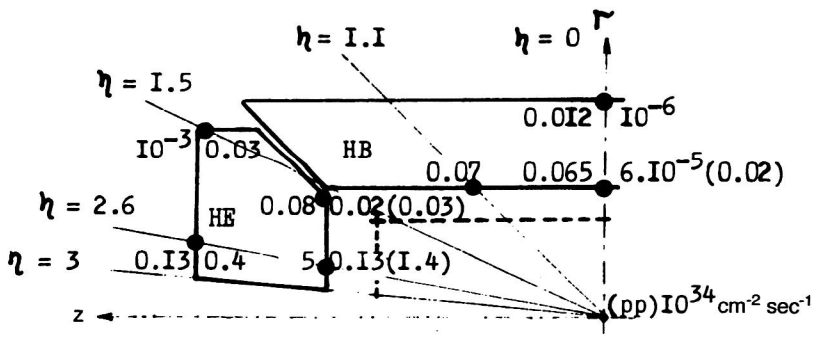

FIG. 11. Comparison of radiation loads in the hadron calorimeter of the CMS. The inner numbers are our estimates (see Sec. 1), the outer ones were calculated in Ref. 30, and the numbers in parentheses were calculated in Ref. 31.

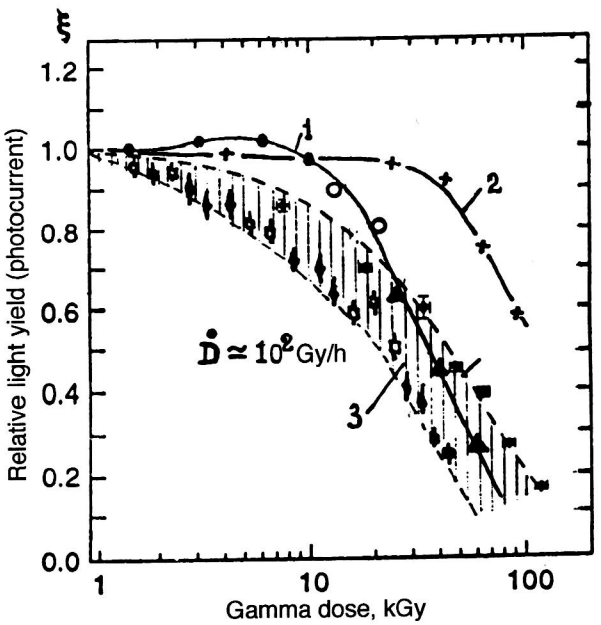

FIG. 12. Dependence of the light yield on the radiation dose: (*1*) samples of standard scintillator;[63,78] (*2*) BCF91A samples;[78] (*3*) calorimeter modules using SCSN81+BCF91A according to the data of Ref. 30.

where $D\sim 2$ Gy/h. The coefficients K_3 (Table IX) were not taken into account, and so the distribution of the relative light yield (curve 1 in Fig. 13) does not correspond to reality.

The statement[30] that the light yield is larger where the "scintillator damage" (ξ) is larger is erroneous. The value of ξ is significantly affected by radiation-induced oxidation (via D), and also by the contribution of other particles, for example, neutrons and fragments, to the dose. For some reason, in Ref. 30 the load is associated only with minimally ionizing particles.

The idea that the large change of the energy resolution in the first few layers of the forward calorimeter (HE) can be corrected by creating a pseudoelement in η and Z with autonomous electronics is based on clearly erroneous initial premises. In fact (Fig. 14), the distribution of the relative light yield in Z and η is more or less uniform (owing to K_3), and so a correction may not be required. However, the light losses cannot exceed 10–20%.

TABLE IX. The coefficient k_3 in the resource expression (3.1).

$\dot{D}$, Gy/h	10^2	10^1	10^0	10^{-1}	10^{-2}	10^{-3}	10^{-4}
PS1	1	0.20	0.04	0.01	0.004	0.002	0.001
PS2	1	0.50	0.25	0.10	0.063	0.018	0.015
SCSN81	1	0.40	0.15	0.09	0.050	0.040	0.035
BC404A	1	0.20	0.0	0.03	0.005	0.002	0.002

Even when D_{lim} is increased by a factor of 2 and $\dot{D}$ lowered by a factor of 2.3, the resource is only 2.5–3 months (Fig. 14). Breaks in the detector operation for $\tau \geqslant 500$ h do not save the SCSN81+BCF91A system, because the resource at $\xi=0.8$ is only 16 months (Fig. 15). The HCAL project should not use the products of the Kuraray company. These products can be used in detectors with low loads, i.e., beyond the limits of the radiation-hazard zone shown in Table III.

Cast and extruded PS1 (PS2) scintillators possess good recovery properties.[98] In Fig. 15 we show the cyclical change of the PS1(PS2)+BCF91A system. For a total dose of 150 kGy after 40 months (equivalent to 10 calendar years) the light-yield loss is less than 10% for loads at the start of not 2 but 5 kGy/h. The calculations were performed on the basis of the measurements (Fig. 10) for PS1 (PS2) scintillators. The ageing of BCF91A was not studied. We started from the following assumptions: (a) the radiation hardness of a fiber is higher than for PS (Fig. 12), and so after the first three or four cycles there will not be any change in the light yield due to transparency of the fiber; (b) in later cycles, degradation can arise only as a result of radiation-induced oxidation.

Temperature measurements of BCF91A (Fig. 7) and the "superposition principle" $D_{\text{reg}}(T_{\text{reg}})=D(298\,\text{K})$ at $D=\dot{D}t=\text{const}$ can be used to estimate the time t_w at which the same effect occurs ($\xi=0.95$) as that observed after a considerably shorter time at a higher temperature. Three control points for BCF91A (Fig. 15) and two for the SCSN81+BCF91A system were obtained in this manner. Of course, this is a rough estimate, and so radiation studies of spectrum-shifting fibers in modules are absolutely necessary.

Therefore, in the hadron calorimeter of the CMS it is necessary to use a cast or extruded scintillator made of inex-

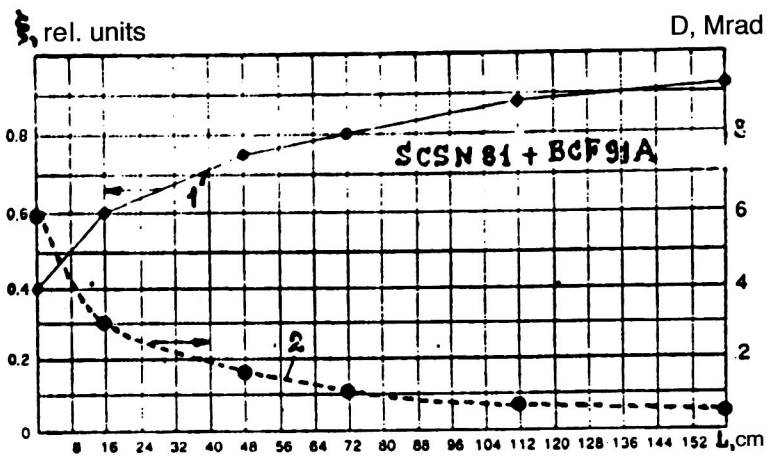

FIG. 13. (*1*) Longitudinal (in Z, Fig. 11) distribution of the light yield and (2) dose inside the HE calorimeter of the CMS according to the data of Ref. 30.

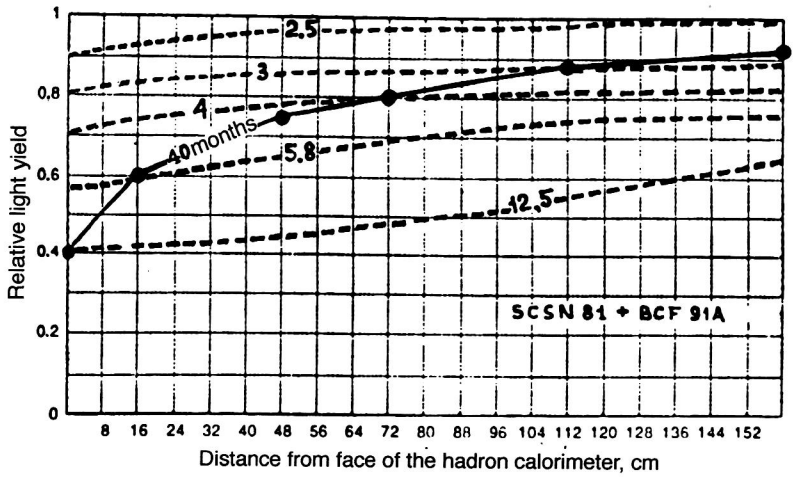

FIG. 14. Longitudinal distribution of the relative light yield of the HE calorimeter of the CMS. The solid line is from Ref. 30, and the dashed lines are our estimates from Fig. 12 and Table IX.

pensive, commercial polystyrene[92] with the condition that the LHC will be shut down (i.e., the beam is turned off) every 2 months for at least 24 hours.

The ECAL resource. It has been decided to use $PbWO_4$ scintillating crystals in the ECAL electromagnetic calorimeter of the CMS.[31] The radiation physics and chemistry of such systems differ considerably from those for organic scintillators, and so they cannot be studied within the narrow scope of the present review.

The periodic shutdown of the beam needed for HCAL will, of course, affect all the CMS detectors. Therefore, study of the spontaneous recovery of $PbWO_4$ is very important. All the recent results of radiation studies of $PbWO_4$ have been systematized in Ref. 107. The practical conclusion was given in Ref. 45. We reproduce it here in Fig. 16 with our comments (shaded region).

Even a cursory review of the studies cited in Ref. 107 shows that different $PbWO_4$ samples have a large spread of light yields after irradiation which does not always fall within the allowed 10% light loss. Figure 16, which shows the data for a single sample (No. 153 with annealing in oxygen), appears to suggest that the radiation dose is unlimited.

However, other studies, for example, Ref. 71, show that in the range 4–8 kGy there is a downward jump which crosses the allowed limit $\xi=0.9$. This is observed in samples with perfect stoichiometry, and of the entire series of samples (and 110 000 of them are needed for ECAL) the lower limit can be realized with a probability of ~90%, and the upper limit with a probability of only ~10%. It is reasonable to take the value ~5 kGy for the limiting allowed dose. Then the resource of the $PbWO_4$ system can be determined from (3.1) with constant uncertainty coefficient K_3 ~2. Apparently, D_{lim} does not depend on D in the case of inorganic crystals.

The resource of continuous irradiation of the forward part of the electromagnetic calorimeter (EE) is insufficient for the maximum loads of 15–28 Gy/h (Fig. 1). It is known that $PbWO_4$ undergoes a complete and rapid recovery of its transparency at low doses (2–3 Gy). At doses of 4–8 kGy the data on the spontaneous recovery of $PbWO_4$ are insufficient. Multi-cycle irradiations of crystals under working conditions, including at small loads of $\sim 10^{-1}$ Gy/h in EB, are just as important as the irradiation of organic scintillators. The use of the data obtained at $D=157$ Gy/h for a real load of 15–0.1 Gy/h in the case of $PbWO_4$ is also not completely correct.

The possibility of constructing heterogeneous electromagnetic calorimeters with energy resolution as good as that in $PbWO_4$ ($\sigma/E \sim 15\%/\sqrt{E}$) by using heavy (with the addition of lead tetraphenyl) polystyrene scintillators was discussed in Ref. 108. Although a radiation hardness of 20 kGy was obtained at a very high load of 187.2 Gy/h even after all the recovery processes, after a dose of less than 3 kGy there

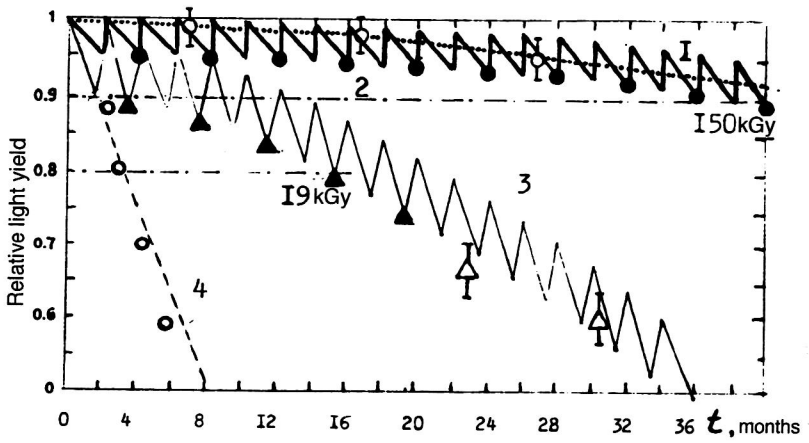

FIG. 15. Decrease of the relative light yield in the HE calorimeter of the CMS (the point $L'=0$, Fig. 13) in cyclical irradiation with recovery: (*1*) BCF91A (⊕ are the estimates from temperature measurements; see Fig. 7); (*2*) PS2 (● are experimental points; see Fig. 10); (*3*) SCSN81+BCF91A (▲ are experimental points; see Fig. 10; and △ is the estimate from temperature measurements); (*4*) SCSN81+BCF91A without recovery (see Fig. 12).

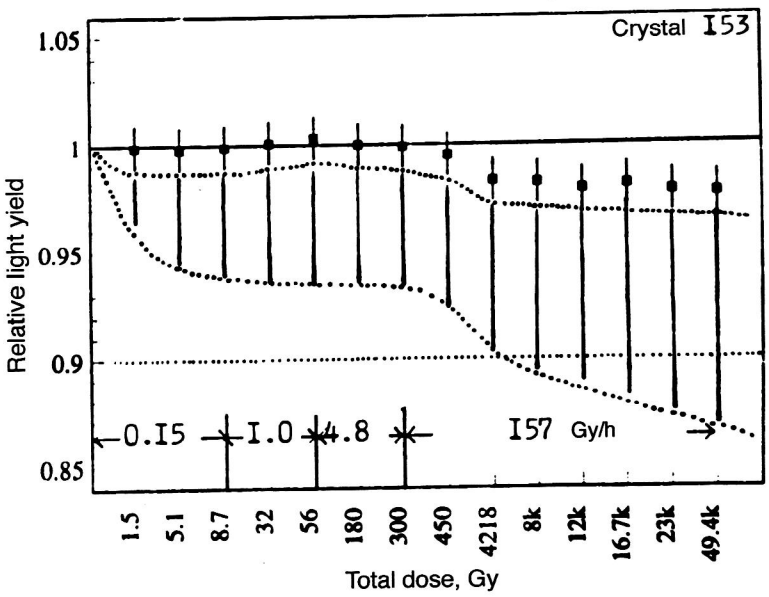

FIG. 16. Change of the light yield of $PbWO_4$ samples right after irradiation: ■ are the experimental points for the best sample, No. 153, annealed in oxygen[34] (the shaded region shows the spread of the experimental data for similar samples).

was still complete spontaneous recovery of all the optical characteristics in thin (thickness 1.1 mm) samples. The introduction of high concentrations of organic metallic impurities (>30%) into PS scintillators lies at the leading edge of the technology for casting under pressure.

Further improvement of the energy resolution of ECAL might be achieved by using heavy scintillators prepared by the other methods discussed in Ref. 108. However, as the authors of that study remark, it will be necessary to realize the periodic irradiation and recovery regime suggested in Refs. 6 and 113 in order to obtain a specified radiation resource.

The HF resource. The largest radiation loads in the CMS occur at the forward calorimeter HF (Fig. 1). The collaboration (see Ref. 44) was forced to use quartz light guides, which have a radiation hardness of order 1 GGy (Ref. 112). However, this causes the calorimeter to have very low energy resolution ($\sigma/E \sim 150\%/\sqrt{E}$), because Čerenkov radiation is detected. If it can be shown that scintillating fibers possess good spontaneous recovery, then their use instead of quartz fibers would allow the resolution to be raised by a factor of 10, and the cost of the calorimeter would be reduced considerably. We note that breaks in the irradiation of the HF calorimeter can be obtained not only by shutting down the LHC, but also by moving the two half-cylinders far apart.

CONCLUSION

The trend in physics is obviously to increase the beam energy and luminosity (especially for AA interactions), both at existing colliders and in other projects planned for the more distant future.[109] This means that detectors must operate under ever more severe radiation conditions. The requirements on the calculations of dose loads are becoming more stringent. The methodology of experiments in radiation physics will approach the conditions of actual use. Comprehensive dosimetric monitoring will be created. The statistical analysis of the reliability of objects on the basis of limited information[110] will allow reliable predictions of detector resources to be made. Such analyses should be performed for all the LHC detector setups, as we proposed earlier in Ref. 64. At present there is no guarantee that the given resources will withstand the projected luminosity of the LHC.

This review of radiation studies of scintillators has convincingly shown that the scintillator resource can be raised only by coordinating irradiation runs and planned breaks. Materials which rapidly and completely recover their original properties during the break time must be used. The lifetime of a material is affected by the operating mode of the collider: the duration of the irradiation runs and the break frequency, the functional time dependence of the luminosity, and the time for startup and circulation of the beams. The sizes of the radiation loads can also be affected by the construction features of the collider: the location of scrapers and collimators near the detector, the dimensions and configuration of the vacuum chamber on segments inside the detector setup, and so on. These questions will determine the strategy for the future operation of colliders and detectors.[111]

[1)]W, mJ/g·sec=D, or Gy/sec (1 Gy=100 rad).

[2)]While this paper was being prepared for publication, such studies became known to us. The results will be published in JINR Brief Communications in 2000.

[1]C. Newman-Holmes, FERMILAB Conf.-96/218E, Fermilab, Batavia (1994).
[2]K. A. Mciel, FERMILAB Conf.-97/214E, CDF and DØ, 1997, Fermilab, Batavia (1997); in *Proceedings of the Second Intern. Conf. on Physics and CP Violation*, Honolulu, Hawaii, 1997.
[3]CMS Technical Proposal, CERN/LHCC-94-32, LHCC/P-1, CERN, Geneva (1994).
[4]ATLAS Technical Proposal, Gen.-Purp. *pp* Exp., LHC CERN-94-43, CERN, Geneva (1994).
[5]Y. Sirois and R. Wigmans, Nucl. Instrum. Methods Phys. Res. A **240**, 262 (1985).
[6]L. N. Zaĭtsev, Nov. OIYaI No. 4, 25 (1996) [in Russian].
[7]N. V. Mokhov, Fiz. Élem. Chastits At. Yadra **18**, 960 (1987) [Sov. J. Part. Nucl. **18**, 408 (1987)].

[8] L. N. Zaĭtsev, *Radiation Effects in Accelerator Structures* [in Russian] (Énergoatomizdat, Moscow, 1987).
[9] I. L. Azhgireĭ and N. V. Mokhov, Preprint 90-132 ORI, IHEP, Protvino (1990) [in Russian].
[10] K. Hahn and J. Ranft, Phys. Rev. D **41**, 1463 (1990).
[11] B. V. Vasilishin, L. N. Zaĭtsev, and I. M. Petoyan, Preprint R16-7036, JINR, Dubna (1974) [in Russian].
[12] L. N. Zaĭtsev *et al.*, Report 16-85-710, JINR, Dubna (1985) [in Russian].
[13] L. N. Zaĭtsev, A. E. Syreĭshchikov, and V. I. Tsovbun, Report 16-87-921, JINR, Dubna (1987) [in Russian].
[14] A. E. Syreĭshchikov, Dissertation, Moscow Engineering Physics Institute (1988) [in Russian].
[15] M. Huhtinen, A. Rubbia, and P. A. Aarnio, Nucl. Instrum. Methods Phys. Res. A **351**, 236 (1994).
[16] A. Fassò *et al.*, CERN TIS 93-08 CF, CERN, Geneva (1993); CERN TIS RP 168, CERN, Geneva (1986).
[17] A. I. Bondarenko *et al.*, Preprint R1-96-447, JINR, Dubna (1996) [in Russian].
[18] A. I. Bondarenko *et al.*, Preprint R1-97-99, JINR, Dubna (1997) [in Russian].
[19] L. R. Kimel' *et al.*, Preprint R16-3514, JINR, Dubna (1967) [in Russian].
[20] T. A. Gabriel and R. T. Santoro, Nucl. Instrum. Methods **99**, 5 (1972).
[21] V. A. Grigor'ev, L. N. Zaĭtsev, I. B. Issinskiĭ *et al.*, Preprint R16-6720, JINR, Dubna (1972) [in Russian].
[22] V. A. Grigor'ev, Dissertation, Moscow Engineering Physics Institute (1973) [in Russian].
[23] L. G. Beskrovnaya and M. M. Komochkov, Report R16-287-304, JINR, Dubna (1987) [in Russian].
[24] G. Stevenson, CERN 90-10, Vol. 3, p. 566 (1990).
[25] P. A. Aarnio and M. Huhtinen, Nucl. Instrum. Methods Phys. Res. A **336**, 98 (1993).
[26] A. Ferrari and P. Sala, Nucl. Instrum. Methods Phys. Res. B **71**, 412 (1992).
[27] A. Fassò *et al.*, Nucl. Instrum. Methods Phys. Res. A **332**, 459 (1993).
[28] M. Huhtinen and P. A. Aarnio, Nucl. Instrum. Methods Phys. Res. A **336**, 545 (1993).
[29] L. N. Zaĭtsev, Fiz. Élem. Chastits At. Yadra **11**, 525 (1980) [Sov. J. Part. Nucl. **11**, 201 (1980)].
[30] HCAL Project, CERN/LHCC 97-31, CMS TDR 3, CERN, Geneva (1997).
[31] ECAL Project, CERN/LHCC 97-33, CMS TDR 4, CERN, Geneva (1997).
[32] C. D'Ambrosio, T. Gis *et al.*, CERN-PPE/96-65, CERN, Geneva (1996).
[33] C. D'Ambrosio *et al.*, Nucl. Instrum. Methods Phys. Res. A **332**, 134 (1993).
[34] C. Goesling, in *Proceedings of the Conf. BEAUTY '95*, Oxford, 1995, p. 187.
[35] M. Huhtinen, CERN CMS TN/96-057, CERN, Geneva (1996).
[36] L. N. Zaĭtsev *et al.*, in *Proceedings of the Sixth European Particle Accelerator Conf.*, Stockholm, 1998, p. 42.
[37] D. L. Broder, L. N. Zaĭtsev *et al.*, *Concrete in the Shielding of Nuclear Reactors* [in Russian], 2nd ed. (Atomizdat, Moscow, 1973).
[38] T. A. Speranskaya and L. I. Tarutina, *Optical Properties of Polymers* [in Russian] (Leningrad, Khimiya, 1976).
[39] V. K. Milinchuk *et al.*, *Macroradicals* [in Russian] (Moscow, Khimiya, 1980).
[40] *Handbook on the Radiation Stability of Organic Materials* [in Russian] (Énergoatomizdat, Moscow, 1986).
[41] L. G. Khamidova *et al.*, Khim. Vys. Énerg. **17**, No. 2, 124 (1983) [in Russian].
[42] L. G. Khamidova *et al.*, Khim. Vys. Énerg. **21**, No. 5, 404 (1987) [in Russian].
[43] E. Yu. Astakhov *et al.*, Vysokomol. Soedin., Ser. A **30**, 702 (1988) [in Russian].
[44] E. Yu. Astakhov *et al.*, Vysokomol. Soedin., Ser. A **30**, 2580 (1988) [in Russian].
[45] I. M. Barkalov, A. M. Zanin *et al.*, Preprint 67-90, Chemical Physics Institute of the USSR Academy of Sciences, Chernogolovka (1990) [in Russian].
[46] V. G. Vasil'chenko *et al.*, No. 3, 58 (1996) [Instrum. Exp. Tech.].
[47] C. Kennedy *et al.*, IEEE Trans. Nucl. Sci. **NS-37**, 144 (1990).
[48] A. D. Bross *et al.*, FERMILAB-Pub-91/54, Fermilab, Batavia (1991).
[49] C. Zorn *et al.*, Nucl. Instrum. Methods Phys. Res. A **276**, 58 (1989).
[50] C. Zorn *et al.*, Nucl. Instrum. Methods Phys. Res. A **273**, 108 (1988).
[51] C. Zorn *et al.*, IEEE Trans. Nucl. Sci. **NS-37**, 487 (1990).
[52] C. D'Ambrosio *et al.*, CERN-PPE/90-96, CERN, Geneva (1990).
[53] R. L. Clough, P. A. Cahill, and C. L. Renschler, in *Proceedings of the Workshop on Radiation Hardness of Plastic Scintillators*, Tallahassee, Florida, 1990, p. 15.
[54] S. Majewski *et al.*, CERN 89-10, CERN, Geneva (1989).
[55] K. F. Johnson *et al.*, IEEE Trans. Nucl. Sci. **NS-37**, 500 (1990).
[56] V. M. Feygelman *et al.*, Nucl. Instrum. Methods Phys. Res. A **295**, 94 (1990).
[57] J. M. Kauffman and M. A. Aziz, see Ref. 63, p. 29.
[58] S. Majewski *et al.*, Nucl. Instrum. Methods Phys. Res. A **281**, 500 (1989).
[59] V. Senchishin *et al.*, Preprint E13-94-159, JINR, Dubna (1994).
[60] G. I. Britvich, V. G. Vasil'chenko, and V. G. Lapshin, No. 1, 75 (1994) [Instrum. Exp. Tech.].
[61] A. A. Astapov *et al.*, JINR Rapid Commun. No. 3[77], 47 (1996).
[62] A. Asmone *et al.*, Nucl. Instrum. Methods Phys. Res. A **338**, 398 (1994).
[63] V. G. Vasil'chenko *et al.*, No. 4, 42 (1996) [Instrum. Exp. Tech.]; G. Anzivino *et al.*, CERN/PC/LP Note 92-14, CERN, Geneva (1992).
[64] L. N. Zaĭtsev, Report R14-95-104, JINR, Dubna (1995) [in Russian].
[65] O. N. Karpukhin, Usp. Khim. **49**, 1523 (1980) [in Russian].
[66] R. L. Gillen and K. T. Glough, in *Proceedings of the Intern. Symp. on Radiation Degradation of Polymer Radiation Resistant Materials Takasaki*, Japan, 1989.
[67] K. T. Glough and R. T. Gillen, Polym. Degr. Stab. **24**, No. 2, 137 (1989).
[68] E. S. Kempner *et al.*, Polym. Sci.: Part B, Polym. Phys. **24**, 2337 (1986).
[69] R. Eremeev *et al.*, JINR Rapid Commun. No. 2[70]-95, 45 (1995).
[70] A. G. Kotov and V. V. Gromov, *Radiation Physics and Chemistry of Heterogeneous Systems* [in Russian] (Énergoatomizdat, Moscow, 1988).
[71] R. Y. Zhu *et al.*, Nucl. Instrum. Methods Phys. Res. A **376**, 319 (1996); M. Kaiser, Diplomarbeit, University of Dortmund (1998).
[72] A. S. Smolyanskiĭ *et al.*, Dokl. Akad. Nauk SSSR **303**, 416 (1988) [in Russian]; G. Marini *et al.*, CERN 85-08, CERN, Geneva (1985).
[73] I. G. Kaplan and A. M. Miterev, Khim. Vys. Énerg. **19**, No. 3, 208 (1985) [in Russian].
[74] S. Egusa *et al.*, Macromolecules **12**, 939 (1979).
[75] S. Egusa *et al.*, Macromolecules **13**, 171 (1980).
[76] T. Sasuga *et al.*, Polymer J. **30**, 2054 (1989).
[77] T. Sasuga *et al.*, in *Proceedings of the Intern. Symp. on Radiation Degradation of Polymer Radiation Resistant Materials*, Takasaki, Japan, 1989, p. 65.
[78] L. N. Zaĭtsev, Preprint R16-98-59, JINR, Dubna (1998) [in Russian].
[79] V. P. Bishop, K. S. Khamferis, and P. T. Randke, Prib. Nauchn. Issled., No. 4, 83 (1973) [in Russian].
[80] B. A. Briksman and V. K. Milinchuk, Khim. Vys. Énerg. **23**, No. 3, 193 (1989) [in Russian].
[81] N. G. Goleminov and E. A. Kramer-Ageev, At. Energ. **49**, 373 (1980) [At. Energ.].
[82] I. I. Zalyubovskiĭ *et al.*, Prib. Tekh. Éksp. No. 3, 76 (1995) [Instrum. Exp. Tech.].
[83] M. Doyle, *Radiation Chemistry of Macromolecules* [Russ. transl., Atomizdat, Moscow, 1978].
[84] V. G. Vasil'chenko *et al.*, Prib. Tekh. Éksp. No. 5, 85 (1995) [Instrum. Exp. Tech.].
[85] V. D. Bezuglii and L. L. Nagornaya, J. Nucl. Energ. **19**, 490 (1965).
[86] U. Holm and K. Wick, IEEE Trans. Nucl. Sci. **36**, 579 (1989).
[87] O. A. Gunder, Preprint IMK-91-15, Kharkov (1991) [in Russian].
[88] G. I. Britvich *et al.*, Preprint IHEP-91-187, IHEP, Protvino (1991).
[89] P. Bonamy *et al.*, Preprint DphPE 91-03, Saclay (1991).
[90] J. Ernwein, Preprint DphPE 91-14, Saclay (1991).
[91] V. V. Brekhovskikh *et al.*, Prib. Tekh. Éksp. No. 6, 95 (1992) [Instrum. Exp. Tech.].
[92] V. K. Anan'ev *et al.*, Prib. Tekh. Éksp. No. 1, 52 (1998) [Instrum. Exp. Tech.].
[93] É. R. Klinshpont, V. P. Kiryukhin, and V. K. Milinchuk, Vysokomol. Soedin., Ser. A **22**, 1754 (1980) [in Russian].
[94] D. S. Sanditov and G. M. Bartenev, *Physical Foundations of Disordered Structures* [in Russian] (Nauka, Novosibirsk, 1982).
[95] V. G. Vasil'chenko *et al.*, Prib. Tekh. Éksp. No. 5, 67 (1996) [Instrum. Exp. Tech.].
[96] V. S. Datsko, Prib. Tekh. Éksp. No. 3, 43 (1996) [Instrum. Exp. Tech.].
[97] All-Union State Standard 170380-79, 170387-79 [in Russian] (Izd. Standartov, Moscow, 1979).

[98] L. N. Zaitsev, A. A. Astapov, V. A. Krasnov *et al.*, in *Proceedings of the Sixth Conf. on Advanced Technology*, Como, Italy, 1998.
[99] S. V. Afanas'ev *et al.*, JINR Brief Commun. No. 7 [81]-97, JINR, Dubna (1997).
[100] M. D. Shafranov, Preprint D13-97, JINR, Dubna (1997) [in Russian].
[101] L. Ya. Zhil'tsova *et al.*, Opt. Spektrosk. **28**, 942 (1970) [Opt. Spectrosc. (USSR)].
[102] L. Ya. Zhil'tsova *et al.*, Zh. Prikl. Spektrosk. **15**, 255 (1971) [in Russian].
[103] A. D. Bross and A. Pla-Dalmau, IEEE Trans. Nucl. Sci. **NS-39**, 1199 (1992).
[104] A. Pla-Dalmau *et al.*, FERMILAB-Pub-95/278, Fermilab, Batavia (1995).
[105] L. A. Andryushchenko and B. V. Grinev, Prib. Tekh. Éksp. No. 1, 52 (1998) [Instrum. Exp. Tech.].
[106] G. I. Britvich *et al.*, Prib. Tekh. Éksp. No. 4, 50 (1998) [Instrum. Exp. Tech.].
[107] E. Auffray *et al.*, Nucl. Instrum. Methods Phys. Res. A **402**, 75 (1998).
[108] G. I. Britvich *et al.*, Prib. Tekh. Éksp. No. 5, 57 (1998) [Instrum. Exp. Tech.].
[109] A. M. Baldin and A. D. Kovalenko, JINR Rapid Commun. No. 3[77]-96, 5 (1996).
[110] Yu. F. Burtaev and V. A. Ostreĭkovskiĭ, *Statistical Analysis of the Reliability of Objects on the Basis of Limited Information* [in Russian] (Énergoatomizdat, Moscow, 1995).
[111] L. N. Zaitsev, in *Proceedings of the Seventeenth Intern. Conf. on High Energy Accelerators*, Dubna, 1998.
[112] V. B. Gavrilov *et al.*, Prib. Tekh. Éksp. No. 4, 23 (1997) [Instrum. Exp. Tech.].
[113] A. A. Astapov and L. N. Zaitsev, JINR Rapid Commun. No. 5[79]-96, JINR, Dubna (1996)

Translated by Patricia A. Millard